# Crystallography of Fracture Facets in a Near-Alpha Titanium Alloy

V. SINHA, M.J. MILLS, and J.C. WILLIAMS

A faceted initiation site is observed in Ti-6242 alloy for both the cyclic and static-loading test conditions. In this experimental study, the crystallographic orientation of the facets has been determined using the electron backscattered diffraction (EBSD) technique in conjunction with the quantitative tilt fractography in a scanning electron microscope (SEM). Quantitative tilt fractography analysis has been used to determine the spatial orientation of fracture facets. The results indicate that the normal-fatigue (no-dwell) fracture facets are oriented at ~5 deg with respect to the basal plane; the dwell-fatigue fracture facets are oriented at ~10 to 15 deg with respect to the basal plane and the static-loading fracture facets are oriented at ~20 deg with respect to the basal plane. These crystallographic orientation determinations of the fracture facets at the crack-initiation site can be used to obtain an idea about the type of loading that produced them.

## I. INTRODUCTION

FACETS have been observed at the crack-initiation site on the fracture surface of near-$\alpha$ titanium alloys tested under normal-fatigue, dwell-fatigue, and static-loading conditions.[1–5] In order to better understand the crack initiation mechanism, it is important to determine the crystallographic orientation of these fracture facets.

Davidson and Eylon[1] determined the orientations of fracture facets obtained under normal-fatigue (no-dwell) and dwell-fatigue conditions in a colony microstructure IMI 685. They used the electron channeling technique in a scanning electron microscope (SEM) for crystallographic orientation determinations. The facets needed to be electro-polished before being characterized using this technique, and moreover, the spot size for pattern collection was relatively large (~50 $\mu$m).[1]

With advances in the electron backscattered diffraction (EBSD) technique in the last decade, it is possible to obtain the EBSD patterns directly from the fracture facet without the need for electro-polishing them. Another important advantage of the recent EBSD technique over the earlier electron channeling technique is that the spot size for pattern collection is much smaller (~20 nm). Therefore, the EBSD technique can be used to characterize the facets that are smaller in size. Bache *et al.*[3] were able to obtain EBSD patterns from fracture facets in a titanium alloy after lightly etching them. The EBSD analysis provides the crystallographic orientation of the grain through which the fracture facet has been produced. For a complete and accurate determination of the crystallographic orientation of the facets, their spatial orientation (*i.e.,* the orientation in space) also needs to be determined. In the prior work on titanium alloy,[3] it is not clear if the spatial orientation of the facets has been accounted for.

V. SINHA, Research Associate 1-Engineer, M.J. MILLS, McDougal Professor of Engineering, and J.C. WILLIAMS, Honda Chair and Professor, are with the Department of Materials Science and Engineering, The Ohio State University, Columbus, OH 43210. Contact e-mail: sinha.19@osu.edu

Manuscript submitted September 7, 2005.

In several studies on other alloys, the importance of determination of spatial orientation of fracture facets for a complete characterization of crystallography of facets has been discussed.[6,7,8] Davies and Randle have used computer-assisted stereo-photogrammetry to obtain a three-dimensional elevation model of the selected area of the fracture surface.[6] This is combined with EBSD analysis to determine the crystallographic orientation of cleavage facets in steel.[6] Semprimoschnig *et al.* have used a similar methodology to determine the crystallography of cleavage planes in Armco iron.[7] Furthermore, Slavik *et al.* have used EBSD analysis on a metallographic section through the fracture surface coupled with a quantitative tilt fractography technique on the facets to determine the crystallography of the fracture facets in an Al alloy.[8]

In the current work, the spatial orientation of the facet plane in Ti-6242 was determined using a modified version of the quantitative tilt fractography technique of Themelis *et al.*[9] This technique essentially consists of analyzing the fractographs obtained in an SEM at two different tilt angles. Moreover, the EBSD patterns were obtained directly from the fracture facets in an SEM and they were indexed in order to determine the crystallographic orientation of the grains through which the facets had been produced. The crystallographic orientations of the fracture facets are presented as inverse pole figures in which both pieces of information (crystallographic orientation of the grain determined by EBSD analysis and spatial orientation of the facet plane determined by quantitative tilt fractography), obtained in an SEM, are combined.

One of the common microstructural conditions in which Ti-6242 alloy is used in practice is the bimodal microstructure with a reasonably high volume fraction of primary $\alpha$. Though the orientation of dwell-fatigue fracture facet for this microstructure has been determined in earlier studies,[9,10] there is very little work on the orientation determination of normal-fatigue and static-loading fracture facets for this microstructure. The objective of the current study was to determine the crystallographic orientation of the normal-fatigue, dwell-fatigue, and static-loading fracture facets in Ti-6242 alloy that had a bimodal microstructure with a high

volume fraction of primary $\alpha$. The results of this study can lead to an improved understanding of the crack initiation mechanism under different loading conditions.

## II. EXPERIMENTAL PROCEDURES

### A. *Material and Specimens*

The Ti-6Al-2Sn-4Zr-2Mo (+Si) alloy that was used in this study was provided in the form of a pancake forging by Ladish Co. (Cudahy, WI). The as-received alloy had a bimodal microstructure, consisting of primary $\alpha$ grains and transformed $\beta$ regions (Figure 1). A more detailed description of microstructure, macrotexture, and microtexture of the as-received alloy is presented elsewhere.[5] This material had a high level of microtexture that has been shown to correspond to a large dwell life debit in this alloy system.[4] The basic tensile properties of the supplied alloy were as follows: 0.2 pct offset yield strength = 950 MPa, ultimate tensile strength = 1017 MPa, and elongation = 17.6 pct. The tensile tests had been conducted at room temperature under displacement control at an actuator speed corresponding to a strain rate of $\sim 1 \times 10^{-4}$ s$^{-1}$.

The normal-fatigue, dwell-fatigue, and static-loading specimens examined in this investigation are taken from a previously reported work.[5] The normal-fatigue test consisted of continuous cycling at 30 cycles per minute, the dwell-fatigue test consisted of 2-minute dwell at the maximum load in each loading cycle, and the static-loading test consisted of keeping the load fixed throughout the test in a dead-load creep frame. For the characterization work reported in the current study, the selected normal-fatigue and dwell-fatigue specimens had been tested at ~91 pct of yield strength and the static-loading specimen had been tested at ~95 pct of yield strength. As has been described in Reference 5, the initiation site consisted of faceted features for each of these specimens (for example, see Figure 2). The characterization results on the dwell-fatigue fracture facets that were produced at ~95 pct of yield strength have been reported elsewhere,[10] and those results are compared with the results of the current study.

### B. *Approach*

In the current study, the position of the loading axis as well as the facet normal is shown (using inverse pole figures) in the crystal axes system of the grain through which the facet had been produced. A schematic of a facet on the fracture surface of a failed specimen is shown in Figure 3(a). It is possible to indicate the position of any direction (presented as a vector in the sample axes system) in the crystal reference frame for a particular grain by plotting the inverse pole figure. For example, the longitudinal direction (**L**) of the specimen can be shown in the crystal reference frame of a particular grain (Figure 3(b)). In Figure 3(b), **L** has been assumed to align with the [0001] crystal direction of the grain under consideration. Two mutually perpendicular radial directions, **R1** and **R2** (both lie in a plane perpendicular to the **L** direction), can also be shown in an inverse pole figure, as indicated in Figure 3(b). Here, **R1** and **R2** are assumed to align with the $[1\bar{2}\bar{1}0]$ and $[10\bar{1}0]$ crystal directions, respectively, of the grain under consideration. Furthermore, any other direction in the sample reference frame can be shown using an inverse pole figure such as Figure 3(b). This is applicable for a facet normal as well, which is represented by a vector $\mathbf{F} = x\,\mathbf{i} + y\,\mathbf{j} + z\,\mathbf{k}$, where **i**, **j**, and **k** are the unit vectors along the *X*, *Y*, and *Z* axes, respectively; and *x*, *y*, and *z* are the components of **F** along the three axes (Figure 3(a)). The orientation of facet normal (**F**) is indicated schematically in an inverse pole figure in Figure 3(b).

Because of the hexagonal crystal symmetry, 6 equivalent points for each of **R1** and **R2**, and 12 equivalent points for **F** are shown in Figure 3(b). If a unit triangle is used to plot the inverse pole figure, only one point corresponding to

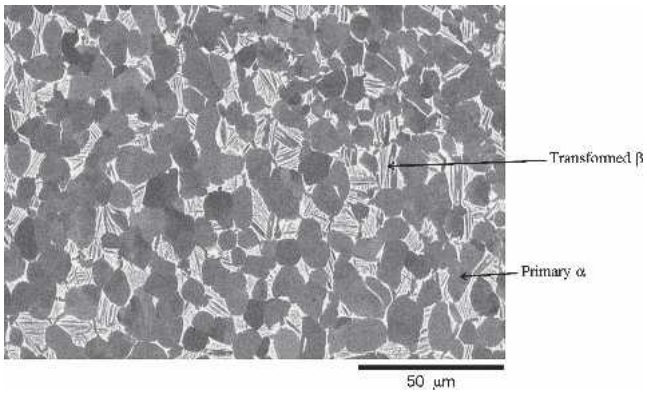


Fig. 1—SEM micrograph of the as-received $\alpha/\beta$ forged Ti-6242 alloy, acquired using a backscattered electron detector.

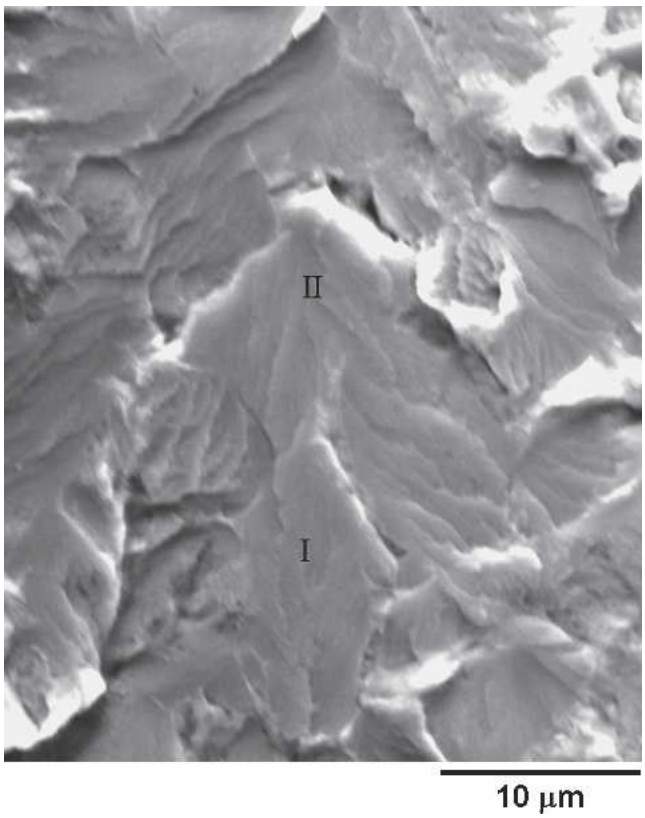


Fig. 2—Faceted initiation site for the normal-fatigue test condition. The crystallographic orientation of the facets labeled "I" and "II" has been determined. SEM stage tilt = 0 deg.

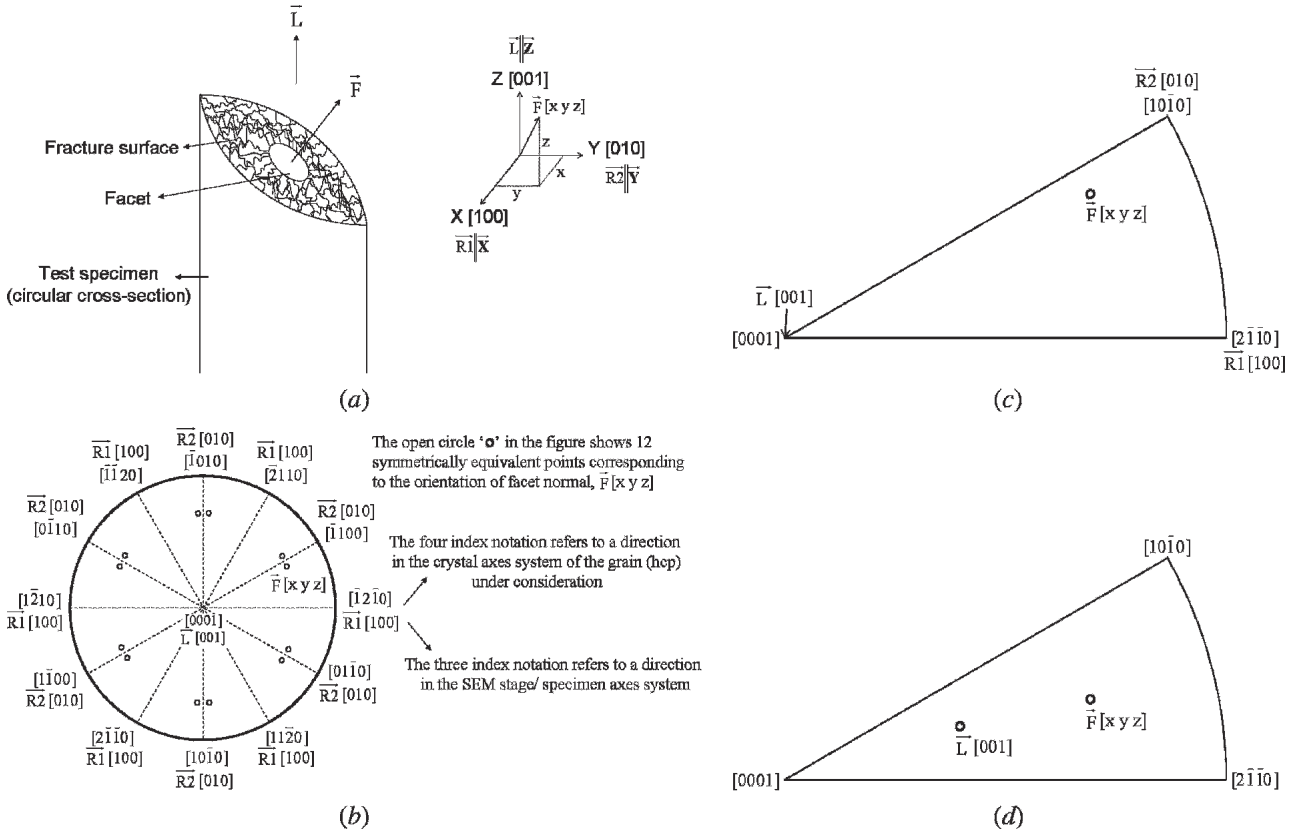


Fig. 3—(*a*) Schematic of an elliptical facet on the fracture surface of a failed test specimen. The facet normal is indicated as **F** and the loading axis for the mechanical tests is indicated as **L**. The Cartesian axes system (SEM stage/specimen axes system), comprising of mutually perpendicular *X*, *Y*, and *Z* axes, is shown in the right. **L** is parallel to the *Z*-axis. Two mutually perpendicular radial directions, **R1** and **R2**, are parallel to *X* and *Y* axes, respectively. (*b*) Inverse pole figure showing the orientation of **L**, **R1**, **R2**, and **F** in the crystal axes system of the grain under consideration. (*c*) Inverse pole figure is plotted using a unit triangle. (*d*) Inverse pole figure is plotted using a unit triangle for a general case when **L** is not parallel to the [0001] crystal direction of the grain under consideration.

each direction will appear in the plot. In Figure 3(c), the positions of **L**, **R1**, **R2**, and **F** are shown using a unit triangle. Similar to Figure 3(b), in Figure 3(c), **L**, **R1**, and **R2** are assumed to align with the [0001], [$\bar{1}$2$\bar{1}$0], and [10$\bar{1}$0] crystal directions, respectively, of the grain under consideration. However, in general, this will not be the case. In Figure 3(d), the orientations of **L** and **F** are shown using a unit triangle for a general case, when **L** is not aligned with the [0001] crystal direction. As will be shown later in this article, two inverse pole figures are plotted for each facet: one indicates the position of loading axis (shown schematically as **L** in Figure 3(d)) and the second one indicates the position of the facet normal (shown schematically as **F** in Figure 3(d)).

### C. *Characterization of Fracture Facets*

The crystallographic orientation of the fracture facets at the crack-initiation site was determined using the quantitative tilt fractography and EBSD techniques in an SEM. The fractured specimens were loaded in the SEM specimen chamber such that their longitudinal direction (*i.e.,* the loading axis during the mechanical tests) is aligned with the electron beam direction of the SEM. The SEM used in the current study is a Philips XL-30 ESEM instrument (FEI Company, Hillsboro, Oregon) that has a field emission gun as the electron source. The spatial orientation of the fracture facets was determined using a quantitative tilt fractography technique in the SEM. This technique involves obtaining SEM images of the facets at two different tilt angles. The analysis of these images provides the normal to the facet plane (**F**) and, thus, helps determine the spatial orientation of fracture facets. The normal to the facet plane is expressed as a vector in the SEM stage axes system. The *X* direction of the SEM stage axes system points to the top of the SEM images, *Y* direction to the left of the SEM images, and *Z* direction is antiparallel to the electron beam direction (Figure 4(a)). The *Y*-axis is also the tilt axis for quantitative tilt fractography as well as EBSD experiments. The quantitative tilt fractography also provides the orientation of the facets with respect to the loading axis. A more detailed description of the tilt fractography technique used in the current study is given elsewhere.[10] This quantitative tilt fractography technique was first applied on a polished smooth specimen. The analysis gave the angle between the *Z*-axis and the normal to the plane of polish as less than 1 deg and, therefore, this technique is believed to be very reliable. Thereafter, this technique was applied on the fracture facets and the results are presented in Section III.

The crystallographic orientation of the grains, through which the fracture facets had been produced, was determined using the EBSD technique in the SEM. The details of this technique have been described elsewhere.[11] A critical step in applying this technique for the analysis of the fracture

facets is the collection of background signal, which is typically collected at a low magnification on the sample being characterized for the case of polished specimens. Due to the unevenness of the fracture surface, a good background signal was difficult to obtain directly from the faceted fracture region. Therefore, the background signal was collected from a polished polycrystalline Ti-6242 specimen at a low magnification (200 times) under the operating conditions (*i.e.,* accelerating voltage, spot size, working distance, and stage tilt) that were subsequently used for the EBSD data collection on the fracture facets. The background subtraction improved the quality of the EBSD patterns obtained from the fracture facets. The operating conditions for EBSD experiments were as follows: accelerating voltage = 20 kV, working distance = 21 mm, and SEM stage tilt = 70 deg. Increasing the number of frames to be averaged for the facet characterization also helped improve the quality of EBSD patterns. The bands in the EBSD patterns so obtained were detected *manually* and the patterns indexed using the OIM analysis computer software (supplied by TSL, Draper, UT) to determine the crystallographic orientation for several locations on a particular fracture facet. The quantitative tilt fractography and the EBSD experiments were completed on a particular facet in one SEM session. Care was taken not to rotate the SEM stage in order to keep the orientation of the fracture facet the same for the two sets of experiments (quantitative tilt fractography and EBSD). The crystallographic orientation of the fracture facets is depicted as the position of facet normal (determined using the quantitative tilt fractography technique as described previously) in the inverse pole figures.

## III. RESULTS

The faceted initiation site obtained for the normal-fatigue test condition (peak stress ~91 pct of yield strength) is depicted in Figure 2. The crystallographic orientation of two adjacent facets (labeled "I" and "II" in Figure 2) was determined. The SEM images of the two facets at 70 deg tilt and at a higher magnification are shown in Figures 4(a) and (b). There are four points each in these images that are marked with an arrow and labeled using letters ("X", "A", "B", and "C"). These four points are used to determine the facet normal using the tilt fractography experiments and analyses. The point labeled "X" serves as the origin for tilt fractography calculations and it is used to calculate the vectors connecting points "A" and "B" (**AB**), and points "B" and "C" (**BC**) at the SEM stage tilt of 0 deg. The cross-product of vectors **AB** and **BC** gives the normal to the facet (**F**) under consideration (Reference 10 provides further details). The four locations (denoted by open circles and labeled using numbers "1" through "4") for which EBSD analyses were carried out on the facets "I" and "II" are shown in Figures 4(a) and (b). In order to indicate the position of the loading axis (**L**) in the crystal axes system, the inverse pole figure is plotted for the [001] direction in the sample reference frame (*i.e.,* SEM stage axes system) and for the crystallographic orientation data obtained at locations labeled "1" through "4" on facets "I" and "II" shown in Figures 4(a) and (b). The [001] direction in the sample reference frame is parallel to the *Z* direction of the SEM stage axes system, and therefore, it is also parallel to the loading axis for the mechanical tests. The position of the loading axis (**L**) in the crystal axes system of the grains through which the two facets are produced is shown in Figure 4(c). It is evident from Figure 4(c) that the loading axis is oriented at ~5 deg from the basal plane normal of the grain through which facet "I" had been produced, whereas the loading axis is oriented less than 5 deg away from the basal plane normal of the grain through which facet "II" had been produced. The position of the facet normal (**F**) in the crystal axes system of the grains through which the two facets are produced is shown in Figure 4(d). The normal for the facets "I" and "II", determined using the tilt fractography technique, are $\mathbf{i} + 1.28\,\mathbf{j} + 26.33\,\mathbf{k}$ and $\mathbf{i} + 0.46\,\mathbf{j} + 21.83\,\mathbf{k}$, respectively (Table I). Here, **i**, **j**, and **k** are the unit vectors along the *X*, *Y*, and *Z* directions (SEM stage axes system), respectively (see the schematic in the left part of Figure 4(a)). Therefore, in order to indicate the position of the normal (**F**) to the facet "I" in the crystal axes system, the inverse pole figure is plotted for the [100 128 2633]* direction in the sample reference frame (*i.e.,* SEM stage axes system) and for the crystallographic orientation data obtained at locations labeled "1" and "2" of facet "I" shown in Figure 4(a). Similarly, in order to indicate the position of normal (**F**) to the facet "II" in the crystal axes system, the inverse pole figure is plotted for the [100 46 2183]* direction in the sample reference frame (*i.e.,* SEM stage axes system) and for the crystallographic orientation data obtained at locations labeled "3" and "4" of facet "II" shown in Figure 4(b). The orientation of the normal (**F**) to facets "I" and "II" is shown in Figure 4(d). It is clear from Figure 4(d) that facet "I" is oriented less than 5 deg away from the basal plane, whereas facet "II" is oriented at ~5 deg with respect to the basal plane.

*It should be noted that each of the three components of the vector representing the facet normal has been multiplied by 100 before entering it for plotting the inverse pole figure, because only the integers (whole numbers) can be entered for plotting inverse pole figures in the OIM analysis software. Multiplying each of the three components of the vector by the same number (100 in the current case) keeps the direction of the facet normal represented by this vector unchanged.

The faceted initiation site obtained for the dwell-fatigue test condition (peak stress ~91 pct of yield strength) is depicted in Figure 5. The crystallographic orientation of two facets, labeled "I" and "II" in Figure 5, was determined. The SEM images of the two facets at 70 deg tilt and at a higher magnification are shown in Figures 6(a) and (b). There are four points each in these images that are marked with an arrow and labeled using letters ("X", "A", "B", and "C"). These four points are used to determine the facet normal using the tilt fractography experiments and analyses, as described earlier. Tilt fractography analysis is used to calculate the vectors connecting points "A" and "B" (**AB**), and points "B" and "C" (**BC**) at the SEM stage tilt of 0 deg. The cross-product of vectors **AB** and **BC** gives the normal to the facet (**F**) under consideration. The eight locations (denoted by open circles and labeled using numbers "1" through "8") for which EBSD analyses were carried out on the facets "I" and "II" are shown in Figures 6(a) and (b). Again, in order to indicate the position of the loading axis

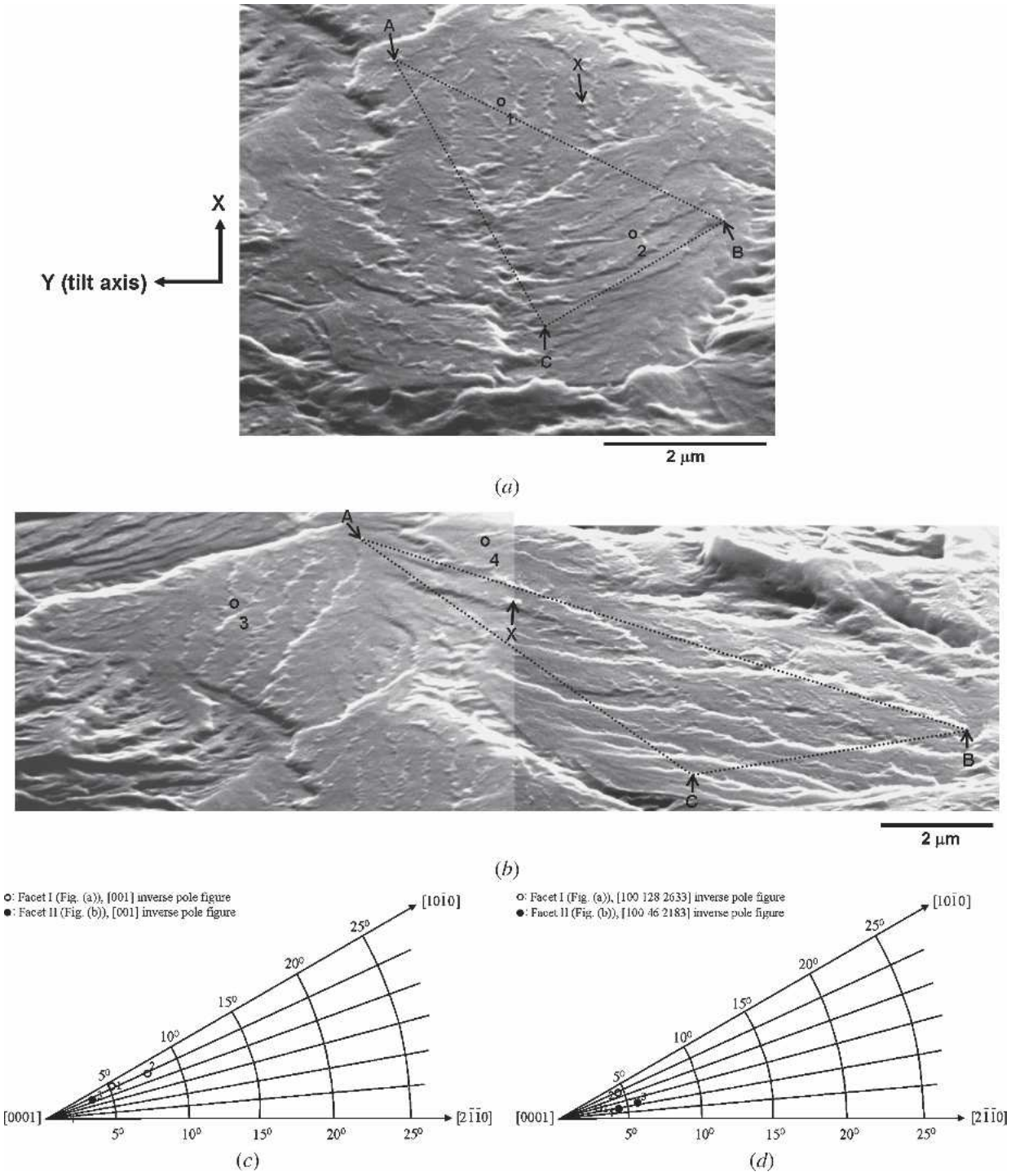


Fig. 4—Crystallographic orientation determination of normal-fatigue fracture facets that have been labeled "I" and "II" in Figure 2. (*a*) SEM image of the facet "I" at 70 deg tilt showing the two locations (denoted by open circles, and labeled "1" and "2") from where the EBSD patterns were obtained and subsequently indexed to determine the crystallographic orientation of the facet. Also shown on the left side of this figure is the schematic representation of the orientation of the SEM stage axes system with respect to the SEM images. The *X*-axis points to the top of the SEM image, *Y*-axis to the left, and *Z*-axis is coming out of the plane of the paper. The *Y*-axis is also the tilt axis for quantitative tilt fractography and EBSD experiments. The orientation of the SEM stage axes system with respect to the SEM images remains the same in all subsequent figures in this article. (*b*) SEM image of the facet "II" at 70 deg tilt showing the two locations (denoted by open circles, and labeled "3" and "4") from where the EBSD patterns were obtained and subsequently indexed to determine the crystallographic orientation of the facet. (*c*) Inverse pole figure showing the position of the loading axis for the two facets based on the EBSD analyses on four locations shown in (*a*) and (*b*). (*d*) Inverse pole figure showing the position of facet normal based on the EBSD analyses on four locations shown in (*a*) and (*b*), and the spatial orientation of the facets. The facet normals, as determined by the quantitative tilt fractography technique, for the facets "I" and "II" are $\mathbf{F} = \mathbf{i} + 1.28\,\mathbf{j} + 26.33\,\mathbf{k}$ and $\mathbf{F} = \mathbf{i} + 0.46\,\mathbf{j} + 21.83\,\mathbf{k}$, respectively (Table I). Here **i**, **j**, and **k** are the unit vectors along *X*, *Y*, and *Z* (SEM stage axes system), respectively. The orientation shown as open circle and labeled "1" in the inverse pole figures (Figures (*c*) and (*d*)) corresponds to the location labeled "1" in (*a*). Similarly, orientations labeled "2", "3", and "4" in inverse pole figures (Figures (*c*) and (*d*)) correspond to the locations in (*a*) or (*b*) that are labeled "2", "3", and "4", respectively.

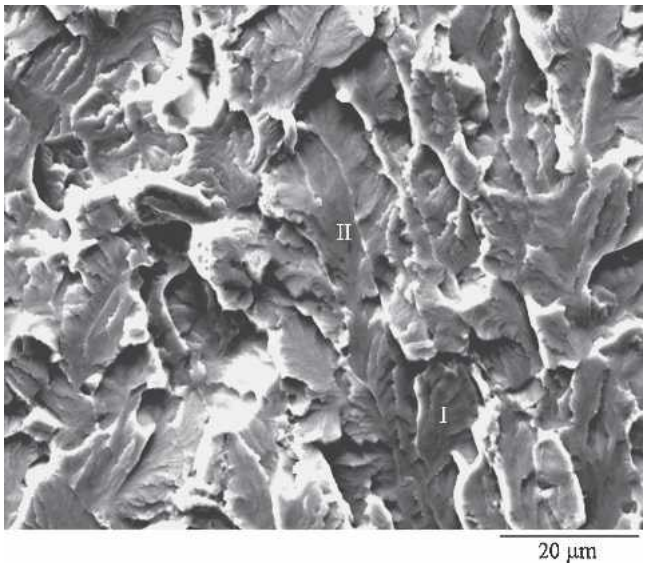


Fig. 5—Faceted initiation site for the dwell-fatigue test condition. The crystallographic orientation of the facets labeled "I" and "II" has been determined. SEM stage tilt = 0 deg.

(**L**) in the crystal axes system, the inverse pole figure is plotted for the [001] direction in the sample reference frame (*i.e.,* SEM stage axes system) and for the crystallographic orientation data obtained at locations labeled "1" through "8" on facets "I" and "II" shown in Figures 6(a) and (b). The position of the loading axis (**L**) in the crystal axes system of the grains through which the two facets are produced is shown in Figure 6(c). It is evident from Figure 6(c) that the loading axis is oriented at ~10 deg from the basal plane normal of the grain through which facet "I" had been produced, whereas the loading axis is oriented at ~15 deg from the basal plane normal of the grain through which facet "II" had been produced. The components of the vectors representing the normal to facets "I" and "II" are shown in Table I. In order to indicate the position of normal (**F**) to the facet "I" in the crystal axes system, the inverse pole figure is plotted for the [−100 −31 1042] direction in the sample reference frame (*i.e.,* SEM stage axes system) and for the crystallographic orientation data obtained at locations labeled "1" through "4" of facet "I" shown in Figure 6(a). Similarly, in order to indicate the position of normal (**F**) to the facet "II" in the crystal axes system, the inverse pole figure is plotted for the [100 −438 2111] direction in the sample reference frame and for the crystallographic orientation data obtained at locations labeled "5" through "8" of facet "II" shown in Figure 6(b). The orientation of the normal (**F**) to facets "I" and "II" is shown in Figure 6(d). It is clear from Figure 6(d) that facets "I" and "II" are oriented at ~15 and ~12 deg, respectively, with respect to the basal plane. We have shown in an earlier study that for the same alloy and microstructure, the loading axis is oriented at 15 to 20 deg from the basal plane normal of the grains through which dwell-fatigue facets had been produced at the peak stress of ~95 pct of yield strength.[10] Furthermore, the dwell-fatigue fracture facets that were produced at ~95 pct of yield strength are observed to be oriented at ~10 deg with respect to the basal plane.[10]

The faceted initiation site obtained for the static-loading test condition (applied stress ~95 pct of yield strength) is shown in Figure 7. The crystallographic orientation of two facets, labeled "I" and "II" in Figure 7, was determined. The SEM images of the two facets at 70 deg tilt and at a higher magnification are shown in Figures 8(a) and (b). There are four points each in these images that are marked with an arrow and labeled using letters ("X", "A", "B", and "C"). These four points are used to determine the facet normal using the tilt fractography experiments and analyses, as described earlier. Tilt fractography analysis is used to calculate the vectors connecting points "A" and "B" (**AB**) and points "B" and "C" (**BC**) at the SEM stage tilt of 0 deg. The cross-product of vectors **AB** and **BC** gives the normal to the facet (**F**) under consideration. The eight locations (denoted by open circles and labeled using numbers "1" through "8") for which EBSD analyses were carried out on the facets "I" and "II" are shown in Figures 8(a) and (b). Once more, in order to indicate the position of the loading axis (**L**) in the crystal axes system, the inverse pole figure is plotted for the [001] direction in the sample reference frame (*i.e.,* SEM stage axes system) and for the crystallographic orientation data obtained at locations labeled "1" through "8" on facets "I" and "II" shown in Figures 8(a) and (b). The position of the loading axis (**L**) in the crystal axes system of the grains through which the two facets are produced is shown in Figure 8(c). It is evident from Figure 8(c) that the loading axis is oriented at ~35 deg from the basal plane normal of the grain through which facet "I" had been produced, whereas the loading axis is oriented at ~45 deg from the basal plane normal of the grain through which facet "II" had been produced. The components of the vectors representing the normal to facets "I" and "II" are shown in Table I. In order to indicate the position of normal (**F**) to the facet "I" in the crystal axes system, the inverse pole figure is plotted for the [−100 256 779] direction in the sample reference frame (*i.e.,* SEM stage axes system) and for the crystallographic orientation data obtained at locations labeled "1" through "4" of facet "I" shown in Figure 8(a). Similarly, in order to indicate the position of normal (**F**) to the facet "II" in the crystal axes system, the inverse pole figure is plotted for the [−100 193 479] direction in the sample reference frame and for the crystallographic orientation data obtained at locations labeled "5" through "8" of facet "II" shown in Figure 8(b). The orientation of the normal (**F**) to facets "I" and "II" is shown in Figure 8(d). It is clear from Figure 8(d) that the facets "I" and "II" are oriented at ~20 deg with respect to the basal plane.

To facilitate the comparison of the orientation data for the facets produced under different loading conditions (normal-fatigue, dwell-fatigue, and static-loading), the orientation of the loading axis (**L**) is shown in one figure (Figure 9(a)) for all the facets characterized in the current study. The orientation of normal (**F**) to the fracture facets that were obtained under different loading conditions is also shown in one figure (Figure 9(b)). Also included in Figure 9 are the orientation data taken from Reference 10 for the dwell-fatigue fracture facets that were produced at ~95 pct of yield strength.

From the quantitative tilt fractography experiments conducted in this work, it is also possible to obtain the

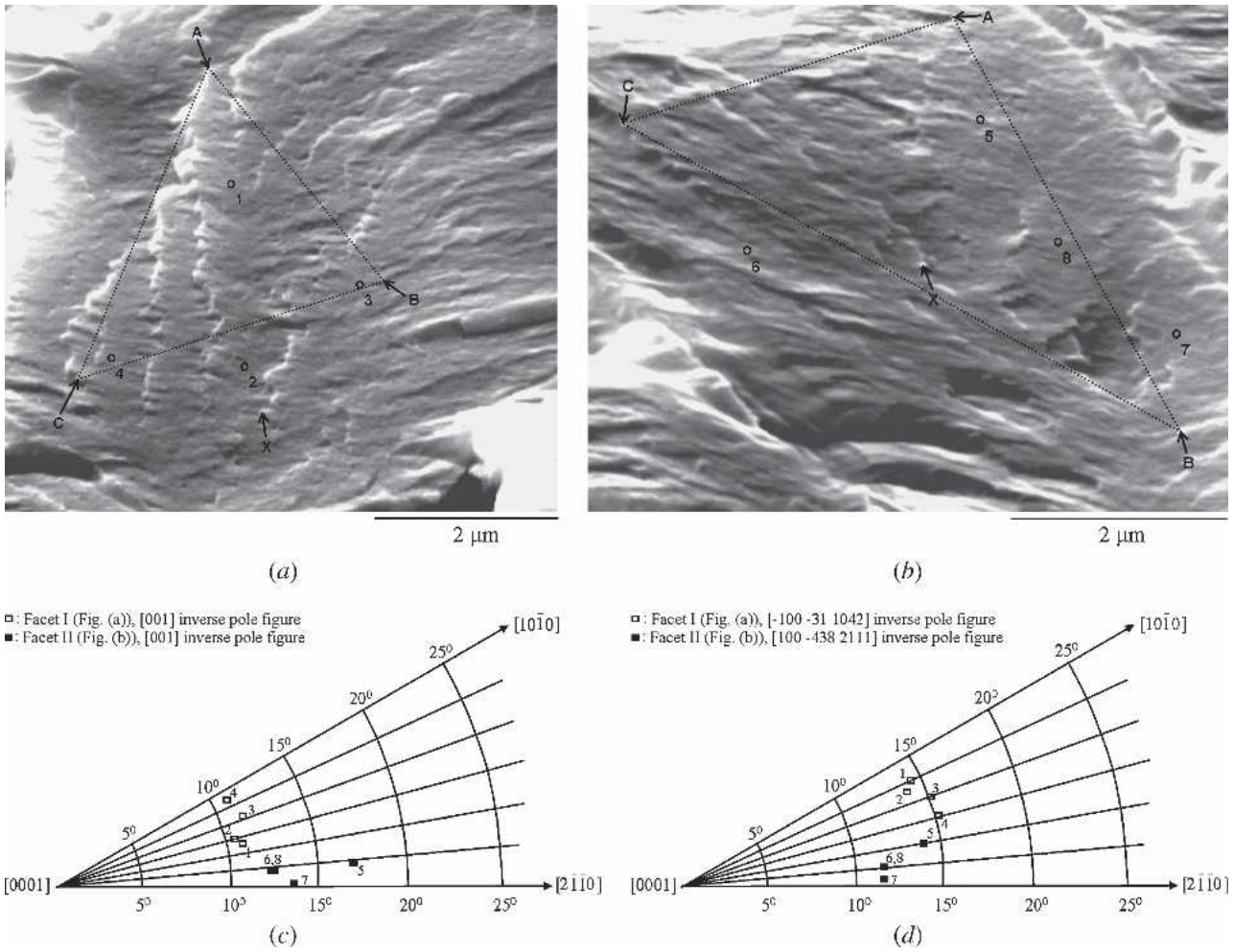


Fig. 6—Crystallographic orientation determination of dwell-fatigue fracture facets that have been labeled "I" and "II" in Figure 5. (*a*) SEM image of the facet "I" at 70 deg tilt showing the four locations (denoted by open circles, and labeled "1", "2", "3", and "4") from where the EBSD patterns were obtained and subsequently indexed to determine the crystallographic orientation of the facet. (*b*) SEM image of the facet "II" at 70 deg tilt showing the four locations (denoted by open circles, and labeled "5", "6", "7", and "8") from where EBSD patterns were obtained and subsequently indexed to determine the crystallographic orientation of the facet. (*c*) Inverse pole figure showing the position of loading axis for the two facets based on the EBSD analyses on eight locations shown in (*a*) and (*b*). (*d*) Inverse pole figure showing the position of facet normal based on the EBSD analyses on eight locations shown in (*a*) and (*b*), and the spatial orientation of the facets. The facet normal, as determined by the quantitative tilt fractography technique, for the facets "I" and "II" are $\mathbf{F} = -\mathbf{i} - 0.31\,\mathbf{j} + 10.42\,\mathbf{k}$ and $\mathbf{F} = \mathbf{i} - 4.38\,\mathbf{j} + 21.11\,\mathbf{k}$, respectively (Table I). The orientations labeled "1", "2", "3", "4", "5", "6", "7", and "8" in inverse pole figures (*c*) and (*d*) correspond to the locations in (*a*) or (*b*) that are labeled "1", "2", "3", "4", "5", "6", "7", and "8", respectively.

angle between the facet normal (**F**) and the loading axis (**L**). The results for the two normal-fatigue, two dwell-fatigue, and two static-loading fracture facets, characterized in the current study, are summarized in Table I. The normal to the normal-fatigue facets shown in Figures 4(a) and (b) is oriented with respect to the loading axis at 4 and 3 deg, respectively (Table I). Moreover, the normal to the dwell-fatigue facets shown in Figures 6(a) and (b) is oriented to the loading axis at 6 and 12 deg, respectively (Table I). For the same alloy and microstructure, the normal to the dwell-fatigue facets, which were produced at ~95 pct of yield strength, is oriented with respect to the loading axis at angles in the range of 12 to 18 deg.[10] On the other hand, the normal to the static-loading facets shown in Figures 8(a) and (b) is oriented with respect to the loading axis at 19 and 24 deg, respectively (Table I). Therefore, the deviation from the loading axis is the smallest for the normal-fatigue facet normal and it is the largest for the static-loading facet normal.

Examples of the EBSD patterns obtained from normal-fatigue, dwell-fatigue, and static-loading fracture facets in the current study are shown in Figures 10(a) through (c). Part of the phosphor screen in our laboratory is damaged and this keeps part of the pattern (labeled "A" in Figures 10(a) through (c)) from being detected. Furthermore, there is another dark region (labeled "B" in Figures 10(a) through (c)), which is caused due to shadowing of the pattern by the adjoining facets and due to the fact that the facet plane is not exactly perpendicular to the electron beam at the SEM stage tilt of 0 deg (as is the case for the specimens polished specifically for EBSD analysis). It should be noted that the size of the dark region labeled "B" increases, in general, for the different test conditions in this order: normal-fatigue, dwell-fatigue, and static-loading (Figures 10(a) through (c)). The angle of facet normal with respect

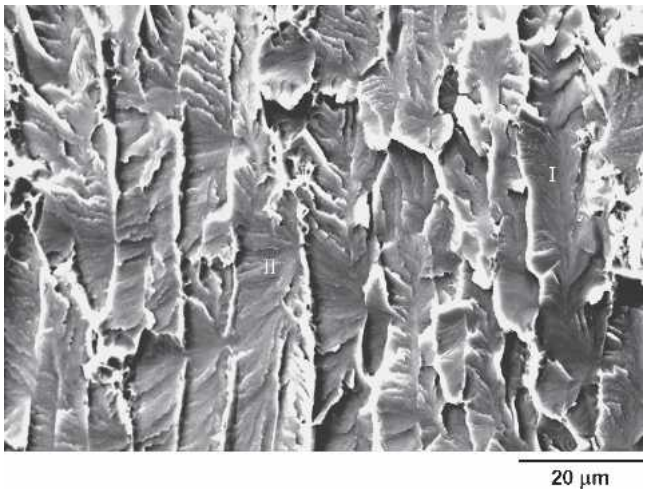


Fig. 7—Faceted initiation site for the static-loading test condition. The crystallographic orientation of the facets labeled "I" and "II" has been determined. SEM stage tilt = 0 deg.

to the loading axis (*i.e.,* *Z*-axis of SEM stage axes system) also increases in the same order (Table I). Thus, a larger angle of inclination of the facet normal from the *Z*-axis of the SEM stage axes system appears to be associated with a larger dark region labeled "B" in the EBSD pattern, which is consistent with the observations of Davies and Randle.[6] The result of the indexing of the patterns presented in Figures 10(a) through (c), using the technique outlined in the current article, is shown in Figures 10(d) through (f). It is clear that in spite of the fact that part of the EBSD patterns is missing, the indexing yields an unambiguous (Figures 10(d) through (f)) and reproducible (Figure 9) crystallographic orientation.

## IV. DISCUSSION

A definite trend in the crystallographic orientation of the fracture facets, at the crack-initiation site, with a change in the type of loading (normal-fatigue, dwell-fatigue, and static-loading) is evident from the results of the current

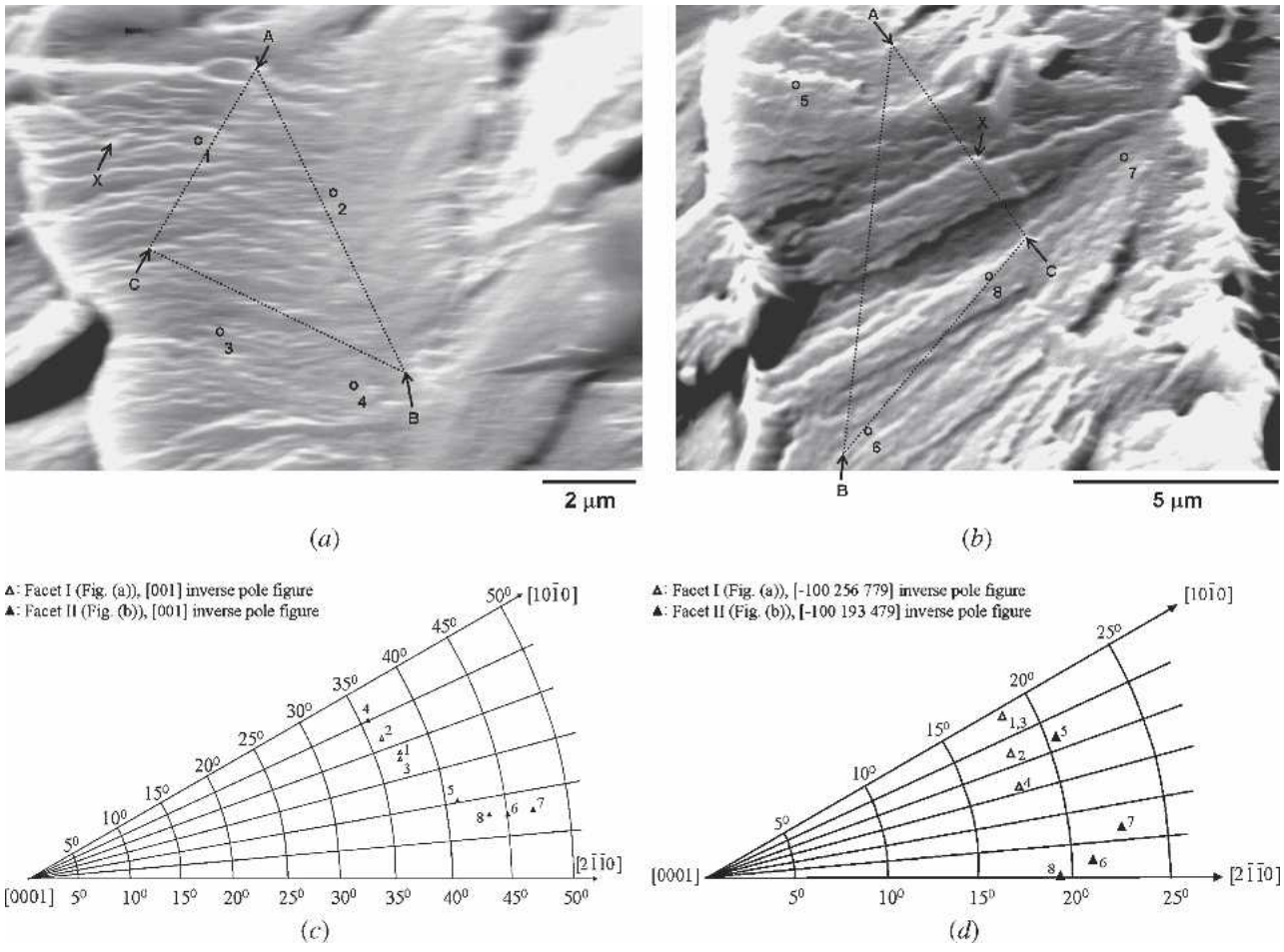


Fig. 8—Crystallographic orientation determination of static-loading fracture facets that have been labeled "I" and "II" in Figure 7. (*a*) SEM image of the facet "I" at 70 deg tilt showing the four locations (denoted by open circles, and labeled "1", "2", "3", and "4") from where the EBSD patterns were obtained and subsequently indexed to determine the crystallographic orientation of the facet. (*b*) SEM image of the facet "II" at 70 deg tilt showing the four locations (denoted by open circles, and labeled "5", "6", "7", and "8") from where EBSD patterns were obtained and subsequently indexed to determine the crystallographic orientation of the facet. (*c*) Inverse pole figure showing the position of loading axis for the two facets based on the EBSD analyses on eight locations shown in (*a*) and (*b*). (*d*) Inverse pole figure showing the position of facet normal based on the EBSD analyses on eight locations shown in (*a*) and (*b*), and the spatial orientation of the facets. The facet normal, as determined by the quantitative tilt fractography technique, for the facets "I" and "II" are $\mathbf{F} = -\mathbf{i} + 2.56\,\mathbf{j} + 7.79\,\mathbf{k}$ and $\mathbf{F} = -\mathbf{i} + 1.93\,\mathbf{j} + 4.79\,\mathbf{k}$, respectively (Table I). The orientations labeled "1", "2", "3", "4", "5", "6", "7", and "8" in inverse pole figures (*c*) and (*d*) correspond to the locations in (*a*) or (*b*) that are labeled "1", "2", "3", "4", "5", "6", "7", and "8", respectively.

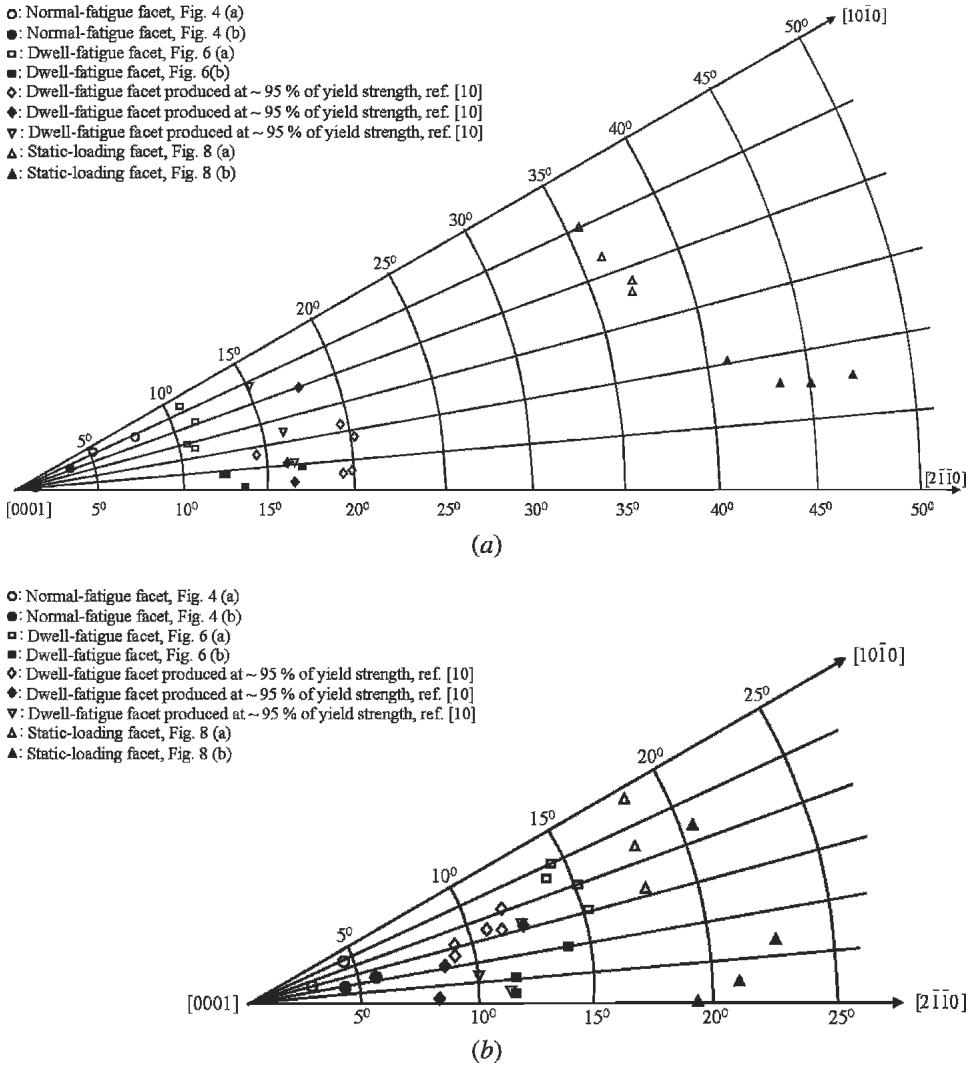


Fig. 9—Inverse pole figures showing the orientation of (*a*) loading axis (**L**), and (*b*) facet normal (**F**) for the facets shown in Figures 4, 6, and 8. The orientations for the dwell-fatigue facets that were produced at a peak stress of ~95 pct of yield strength are taken from Reference 10.

study. The deviation from the basal plane is the smallest for the normal-fatigue fracture facets, it is the largest for the static-loading fracture facets, and it is intermediate for the dwell-fatigue fracture facets (Figure 9(b)). Furthermore, dwell-fatigue fracture facets produced at different peak stresses (~91 and ~95 pct of yield strength) have similar crystallographic orientations (Figure 9(b)). Davidson and Eylon[1] have also characterized the normal-fatigue and dwell-fatigue fracture facets in a colony microstructure IMI 685, although using a different technique (electron channeling technique). They reported that the facets, near the fracture origin, had a pure-basal orientation for the normal-fatigue test condition, whereas they had a near-basal orientation (7 to 15 deg away from the basal plane) for the dwell-fatigue test condition.[1] Therefore, their finding on the trend of variation in the crystallographic orientation of the fracture facets with a change in the type of loading (normal-fatigue *vs* dwell-fatigue) is consistent with the results of the current study, which is conducted on Ti-6242 alloy in a different microstructural condition (bimodal microstructure with a reasonably high volume fraction of primary $\alpha$ (Figure 1)). It is an interesting and new finding of the current study that the static-loading fracture facets are even further away from the basal orientation than the dwell-fatigue facets. The reason for a larger off-basal deviation of dwell-fatigue facets than normal-fatigue facets and of static-loading facets than dwell-fatigue facets is currently not well understood. However, it is worthwhile to mention that the spatial orientation of the facets has been determined for an area of the facet that is enclosed by dashed lines joining the points ''A'', ''B'', and ''C'' in Figures 4(a), 4(b), 6(a), 6(b), 8(a), and 8(b). Determining the facet normal (**F**) for an area significantly smaller than what has been analyzed in the current study (*i.e.,* area enclosed by dashed lines joining the points ''A'', ''B'', and ''C'' in Figures 4(a), 4(b), 6(a), 6(b), 8(a), and 8(b)) would require acquisition and analyses of the SEM images at two different tilt angles at significantly higher magnifications. However, the resolution of these images gets reduced to an extent that it does not permit a reliable determination of facet normal. Therefore, in the current study, the facet area for spatial orientation determination is much larger than the area (spot size of

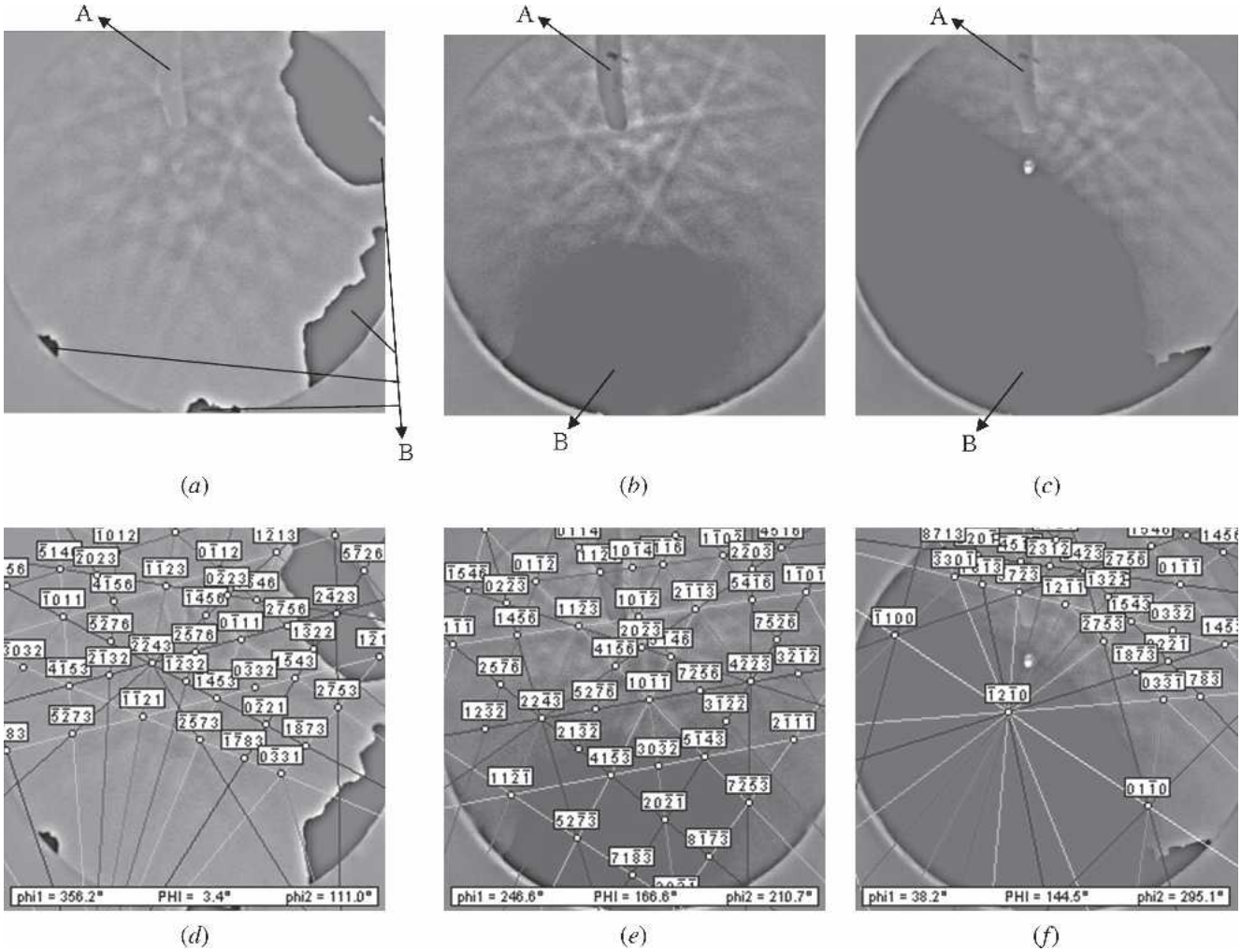


Fig. 10—Examples of the EBSD patterns obtained from the facets produced under different test conditions: (*a*) normal-fatigue, (*b*) dwell-fatigue, and (*c*) static-loading. Part of the patterns is not detected: the region labeled ''A'' in (*a*) through (*c*) is due to the damage in this small part of the phosphor screen, whereas the region labeled ''B'' is due to shadowing of the pattern by the adjoining facets and due to the fact that the fracture facet is not exactly normal to the electron beam at the SEM stage tilt of 0 deg. Even with part of the pattern missing, the indexing yields an unambiguous, correct, and reproducible result. (*d*), (*e*), and (*f*) show the indexing of the patterns shown in (*a*), (*b*), and (*c*), respectively.

electron beam ~20 nm) for EBSD pattern collection. Furthermore, it is apparent from the SEM images of the facets at the stage tilt of 70 deg (Figures 4(a), 4(b), 6(a), 6(b), 8(a), and 8(b)) that the area of the facets for which the facet normal (**F**) has been determined (*i.e.,* the area bound by dashed lines joining the points ''A'', ''B'', and ''C'') is not smooth but consists of steps. Moreover, the height of these steps qualitatively appears to increase (*i.e.,* the roughness of facets increases) in this order: normal-fatigue facets (Figures 4(a) and (b)), dwell-fatigue facets (Figures 6(a) and (b)), and static-loading facets (Figures 8(a) and (b)). This could possibly account for some of the differences in the crystallographic orientation of the fracture facets obtained under different loading conditions (Figure 9(b)), because this depiction of crystallographic orientations is based, in part, on the spatial orientation of the facets that are determined for an area enclosed by dashed lines joining the points ''A'', ''B'', and ''C'' in Figures 4(a), 4(b), 6(a), 6(b), 8(a), and 8(b). In other words, had it been possible to determine the spatial orientation (*i.e.,* facet normal, **F**) of a facet area that was only marginally larger than the area for EBSD pattern collection, the crystallographic orientation of the facets for different test conditions might have had less mismatch than that shown in Figure 9(b). However, more experiments and analyses are needed to confirm this hypothesis. Additional experiments, including the transmission electron microscope (TEM) specimen preparation directly from the fracture facets using the focused ion beam technique and TEM examination of these specimens, are currently underway in our laboratory and the results of this ongoing work are likely to shed some light on this subject.

In any case, the characterization results of the current study suggest that it could be possible to obtain an idea about the type of loading that produced a particular fracture facet at the crack-initiation site by determining its crystallographic orientation using the methodology employed in this work. This is particularly useful for understanding the cause of crack initiation in a component that may be subject to different types of loading (*e.g.,* any two or all three of the normal-fatigue, dwell-fatigue, and static-loading).

**Table I. Summary of Quantitative Tilt Fractography Results**

| Test Condition | Reference Figure | Vector Representing the Facet Normal (**F**) | Angle between Facet Normal (**F**) and Loading Axis (**L**)** |
|---|---|---|---|
| Normal-fatigue (peak stress ~91 pct of yield strength) | Fig. 4(a) | **i*** + 1.28 **j*** + 26.33 **k*** | 4 deg |
| Normal-fatigue (peak stress ~91 pct of yield strength) | Fig. 4(b) | **i** + 0.46 **j** + 21.83 **k** | 3 deg |
| Dwell-fatigue (peak stress ~91 pct of yield strength) | Fig. 6(a) | −**i** − 0.31 **j** + 10.42 **k** | 6 deg |
| Dwell-fatigue (peak stress ~91 pct of yield strength) | Fig. 6(b) | **i** − 4.38 **j** + 21.11 **k** | 12 deg |
| Static-loading (test stress ~95 pct of yield strength) | Fig. 8(a) | −**i** + 2.56 **j** + 7.79 **k** | 19 deg |
| Static-loading (test stress ~95 pct of yield strength) | Fig. 8(b) | −**i** + 1.93 **j** + 4.79 **k** | 24 deg |

*__i__, __j__, and __k__ are the unit vectors along *X*, *Y*, and *Z* (SEM stage axes system), respectively (Fig. 4(a)).

**The fractured specimens were placed in the SEM such that their longitudinal direction (*i.e.,* loading axis during the mechanical tests) is parallel to the *Z*-axis of the SEM stage axes system.

It is relevant to mention that Wagner *et al.*[12] have observed first the formation of intense slip bands, then crack nucleation at these slip bands, and thereafter the small crack propagation along these slip bands during normal-fatigue testing of electropolished Ti-8.6 Al specimens. Wojcik *et al.* have also reported cracking along the slip bands during stage I fatigue crack propagation in Ti-811 alloy.[13] In view of this, it is curious to observe fatigue cracks that initiate in a spatial orientation that corresponds to relatively low resolved shear stress values for basal slip. We have considered this point and believe that it requires considerable elaboration that is beyond the scope of this article, both in terms of content and length. We are conducting additional experiments to elucidate this point. These results will be the subject of a forthcoming article.

Evans and Bache[14] have reported that the fracture facets are oriented at approximately 45 deg to the loading axis when the peak stress for the normal-fatigue test is above yield. On the other hand, when the peak stress for normal-fatigue test is below yield, the fracture facets are approximately perpendicular to the loading axis.[14] In the current study, the peak stress for the normal-fatigue specimen is below yield (~91 pct of yield strength). Therefore, the finding of a near-perpendicular orientation of normal-fatigue fracture facets with respect to the loading axis (Table I) is consistent with the results of Evans and Bache.[14]

## V. SUMMARY AND CONCLUSIONS

In the current study, results of two complementary techniques have been used to determine the crystallographic orientation of fracture facets that are produced at the crack-initiation site under different loading conditions in a Ti-6242 alloy. This technique consists of quantitative tilt fractography analysis to determine the spatial orientation of fracture facets and EBSD analysis to determine the crystallographic orientation of the grains through which fracture facets are produced. The results of the current study show that the deviation of the fracture facets from the basal plane is different for the different test conditions (normal-fatigue, dwell-fatigue, and static-loading), and it changes from the smallest to the largest in the following order: normal-fatigue, dwell-fatigue, and static-loading. The reason for this change in crystallographic orientation with a change in the loading condition is currently not clear, but is the subject of continuing study. Davidson and Eylon have used an earlier electron channeling technique to determine the crystallographic orientation of normal-fatigue and dwell-fatigue fracture facets near the fracture origin,[1] and their results on the relative crystallographic orientation of normal-fatigue and dwell-fatigue fracture facets are consistent with the results of the current study. Their observations[1] serve as an independent check on the overall methodology used to determine the crystallographic orientation of the fracture facets in the current study. Furthermore, an important and new finding of the current work is that the deviation of the static-loading fracture facets from the basal plane is larger than that of the normal-fatigue or dwell-fatigue fracture facets. These results also indicate that the determination of the crystallographic orientation of fracture facets at the crack-initiation site can give us an idea about the type of loading that produced them. This could be useful from a practical standpoint, because this analysis may help determine the cause of crack initiation in a component that is subject to different types of loading in service.

## ACKNOWLEDGMENTS

This research was supported by the Federal Aviation Administration. The authors thank the Technical Monitor, Joseph Wilson, for his encouragement and support of this work. The donation of Ti-6242 pancake forging by Ladish Co. Foundation (Cudahy, WI) is also gratefully acknowledged.

## REFERENCES

1. D.L. Davidson and D. Eylon: *Metall. Trans. A*, 1980, vol. 11A, pp. 837-43.
2. M.R. Bache, H.M. Davies, and W.J. Evans: *Titanium '95: Science and Technology*, University Press, Cambridge, U.K., 1995, pp. 1347-54.

3. M.R. Bache, W.J. Evans, and H.M. Davies: *J. Mater. Sci.*, 1997, vol. 32, pp. 3435-42.
4. A.P. Woodfield, M.D. Gorman, R.R. Corderman, J.A. Sutliff, and B. Yamrom: *Titanium '95: Science and Technology*, University Press, Cambridge, U.K., 1995, pp. 1116-24.
5. V. Sinha, M.J. Mills, and J.C. Williams: *Metall. Mater. Trans. A*, 2004, vol. 35A, pp. 3141-48.
6. P.A. Davies and V. Randle: *J. Microsc.*, 2001, vol. 204, Part 1, pp. 29-38.
7. C.O.A. Semprimoschnig, J. Stampfl, R. Pippan, and O. Kolednik: *Fatigue Fract. Eng. Mater. Struct.*, 1997, vol. 20 (11), pp. 1541-50.
8. D.C. Slavik, J.A. Wert, and R.P. Gangloff: *J. Mater. Res.*, 1993, vol. 8 (10), pp. 2482-91.
9. A.P. Woodfield and J.A. Sutliff: *Microsc. Microanal.*, 1997, vol. 3 (2), pp. 571-72.
10. V. Sinha, M.J. Mills, and J.C. Williams: *J. Mater. Sci.*, in press.
11. S.I. Wright: in *Electron Backscatter Diffraction in Materials Science*, A.J. Schwartz, M. Kumar, and B.L. Adams, eds., Kluwer Academic/Plenum Publishers, New York, NY, 2000, pp. 51-64.
12. L. Wagner, J.K. Gregory, A. Gysler, and G. Lütjering: in *Small Fatigue Cracks*, Proc. 2nd Engineering Foundation Int. Conf./Workshop, Santa Barbara, CA, Metallurgical Society, Warrendale, PA, R.O. Ritchie and J. Lankford, eds., 1986, pp. 117-27.
13. C.C. Wojcik, K.S. Chan, and D.A. Koss: *Acta Metall.*, 1988, vol. 36 (5), pp. 1261-70.
14. W.J. Evans and M.R. Bache: *Int. J. Fatigue*, 1994, vol. 16 (7), pp. 443-52.